

Cite this: *Mater. Horiz.*, 2022, 9, 1089Received 27th July 2021,
Accepted 19th January 2022

DOI: 10.1039/d1mh01186c

rsc.li/materials-horizons

Bright excitonic multiplexing mediated by dark exciton transition in two-dimensional TMDCs at room temperature†

 Shaul Katznelson,^{‡ab} Bar Cohn,^{‡bc} Shmuel Sufrin,^{‡bc} Tomer Amit,^d
 Subhrajit Mukherjee,^{id a} Vladimir Kleiner,^{bc} Pranab Mohapatra,^e Avinash Patsha,^{id e}
 Ariel Ismach,^{id e} Sivan Refaely-Abramson,^d Erez Hasman^{bc} and Elad Koren^{id *abf}

2D-semiconductors with strong light–matter interaction are attractive materials for integrated and tunable optical devices. Here, we demonstrate room-temperature wavelength multiplexing of the two-primary bright excitonic channels (A_b -, B_b -) in monolayer transition metal dichalcogenides (TMDs) arising from a dark exciton mediated transition. We present how tuning dark excitons via an out-of-plane electric field cedes the system equilibrium from one excitonic channel to the other, encoding the field polarization into wavelength information. In addition, we demonstrate how such exciton multiplexing is dictated by thermal-scattering by performing temperature dependent photoluminescence measurements. Finally, we demonstrate experimentally and theoretically how excitonic mixing can explain preferable decay through dark states in MoX_2 in comparison with WX_2 monolayers. Such field polarization-based manipulation of excitonic transitions can pave the way for novel photonic device architectures.

Introduction

Excitons are fundamental optically excited, Coulomb-bound electron–hole pairs in semiconductors. Ever-present, excitons play a major role in the optical properties of reduced

New concepts

In this work, we demonstrate strong wavelength multiplexing of the two-primary bright excitonic channels in MoX_2 based monolayers, exploiting the dark excitation of the A_g -transition. This is realized by control over the out-of-plane component of the excitation electric field, encoding the polarization information into the two bright spectral channels at room temperature. Particularly, substantial out-of-plane excitation is used to generate high energy A_g -excitons, which leads to dominant B_b -emission. In contrast, purely in-plane dipole excitation results in a predominant A_b -emission. We further establish the pivotal role of thermal energy and CB ordering in supporting or suppressing the multiplexing for MoX_2 and WX_2 , respectively. Finally, state of the art *ab initio* GW-BSE calculations were carried out demonstrating a rich excitonic exchange interaction that strongly support the presented PL multiplexing phenomena, temperature dependent PL spectra and the observed deviation between Mo- and W-based TMDCs. Our new findings shine light on the fundamental optical properties of monolayer TMDs, while paving a novel route for TMDs based photonic devices, e.g. spectral bits for optical computing, multifunctional light sources and more.

dimensionality semiconductors such as quantum wells (1D and 2D) and monolayer transition-metal dichalcogenides (TMDs), due to their reduced dielectric screening and significant spatial confinement.^{1–4} In particular, in comparison with other 2D semiconductors, monolayer TMDs feature robust bound excitons with exceptionally large binding energy,^{2–4} making monolayer TMDs an attractive platform for adequate light–matter interaction investigations and nanophotonic applications at room temperature.^{5–8}

Monolayer TMDs, typically presented as MX_2 (where M = Mo, W; X = S, Se), have non-centrosymmetric hexagonal crystal structure, resulting in a direct bandgap at the $\pm K$ valley.^{9,10} In addition, strong spin–orbit coupling (SOC) removes the valence band (VB) and conduction band (CB) spin degeneracy.¹¹ For the former, the spin splitting is on the order of hundreds of meV, spectrally separating two distinct excitonic channels generated from the higher and lower VB, termed the A- and B-excitons, respectively.^{2,12} Compared with its VB counterpart, the CB splitting is considerably smaller- on the scale of a few

^a Nanoscale Electronic Materials and Devices Laboratory, Faculty of Materials Science and Engineering, Technion – Israel Institute of Technology, Haifa 3200003, Israel. E-mail: eladk@technion.ac.il

^b Russell Berrie Nanotechnology Institute, and Helen Diller Quantum Center, Technion – Israel Institute of Technology, Haifa 3200003, Israel

^c Atomic-Scale Photonics Laboratory, Faculty of Mechanical Engineering, Technion – Israel Institute of Technology, Haifa 3200003, Israel

^d Department of Molecular Chemistry and Materials Science, Weizmann Institute of Science, Rehovot 7610001, Israel

^e Department of Materials Science and Engineering, Tel Aviv University, Ramat Aviv, Tel Aviv, 6997801, Israel

^f The Nancy and Stephen Grand Technion Energy Program, Technion – Israel Institute of Technology, Haifa 3200003, Israel

† Electronic supplementary information (ESI) available. See DOI: 10.1039/d1mh01186c

‡ These authors contributed equally.

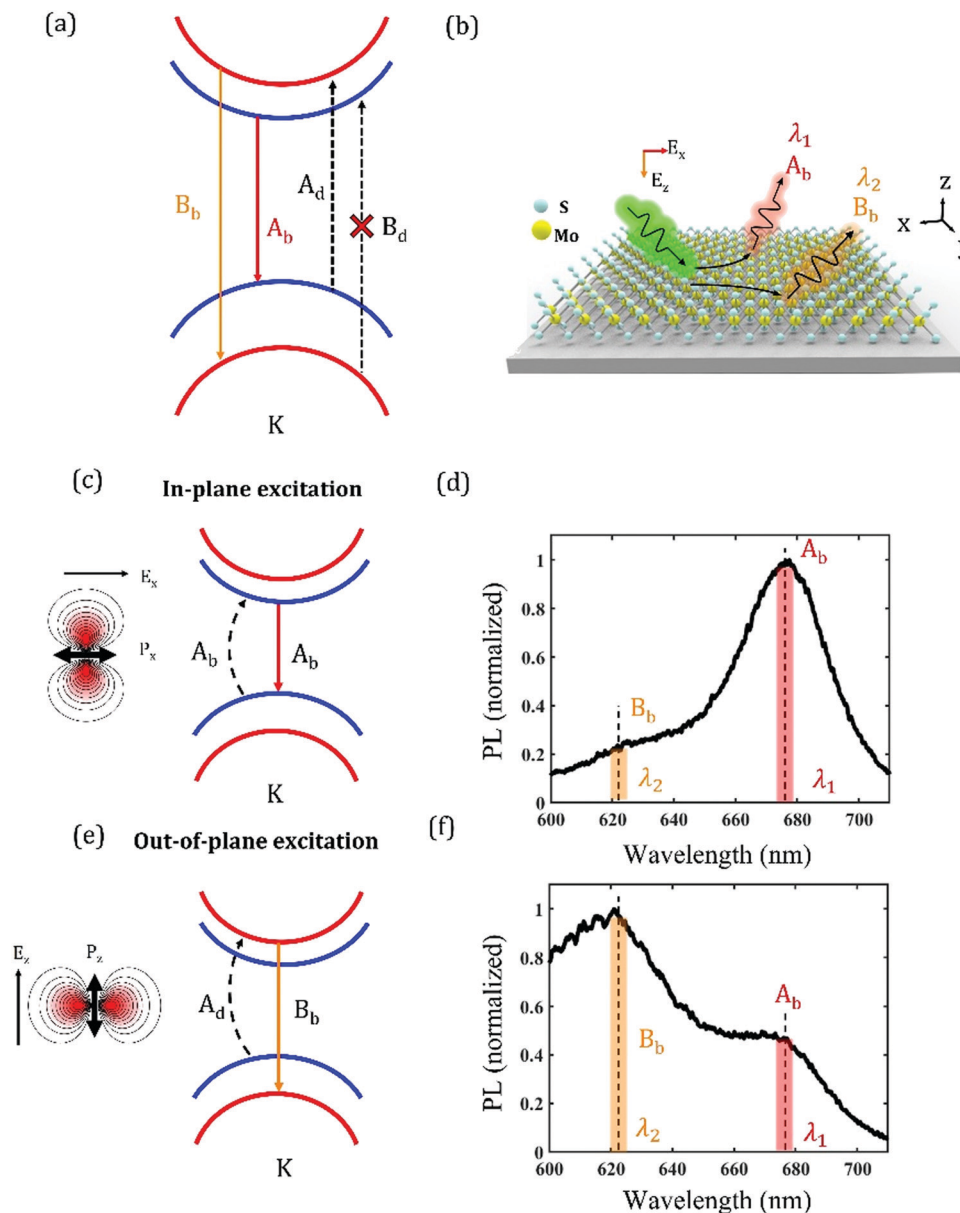


Fig. 1 Photoluminescence selection of A_b - and B_b -exciton in monolayer MoS_2 induced by in- and out-of-plane excitation. (a) – Electronic band structure of monolayer MoS_2 at the K valley. Bands color code represents the spin degree of freedom. The colored (dashed) arrows represent bright (dark) exciton transitions, respectively. (b) Schematic illustration of the A_b - and B_b -exciton wavelength multiplexing in monolayer MoS_2 on Si/SiO₂ substrate. The method is based on tuning the out-of-plane component of the exciting electric field to select exciton channel. (c) In-plane excitation (marked by dashed line A_b) followed by emission from the A_b -excitonic channel marked by the red arrow. On the left, an illustration of an in-plane dipole transition (A_b -) with its radiation profile excited by in plane polarized field. (d) Photoluminescence spectra of MoS_2 excited by mostly in-plane polarized light showing a predominant emission of the A_b -excitonic channel marked by λ_1 . (e) Out-of-plane excitation (marked by the dashed line A_d) followed by B_b -excitonic channel marked by the orange arrow. On the left an illustration of an out-of-plane dipole (A_d -) transition with its radiation profile excited by an out-of-plane polarized field. (f) Photoluminescence spectra of MoS_2 excited through dark exciton results in the predominant emission of the B_b excitonic channel marked as λ_2 .

meV.^{10,13} While small, this splitting governs the optical selection rules, separating the excitonic transition into distinct bright and dark channels with orthogonal transition dipole orientations.^{14,15} Thus, the associated excitonic transitions can be classified as either optically bright A_b -, B_b - or optically dark A_d -, B_d - excitons (Fig. 1a). Note that the brightness of these states is also determined by symmetry and momentum

selection rules as extensively discussed before for this class of materials.^{16–18}

Bright excitons correspond to optically-allowed electron–hole transitions with the same spin orientation. These transitions strongly couple to light *via* in-plane (x - y direction) dipoles,¹⁹ making the A_b -, B_b -channels the dominant features in conventional photoluminescence (PL) spectrum. Interestingly, the main

PL emission channel in TMDs arises from the A_b -exciton,^{2,20} where to date, limited increase of the B_b -exciton emission signal was realized by several factors such as pump intensity,²¹ substrate,²² sample quality,²³ and bright-to-bright exciton mixing²⁴ (see ESI† note 1). Nonetheless, an all-optical way enabling strong modulation between the two bright excitonic channels can pave the way for exciting tunable multi-wavelength devices.

The two low-lying and spin-split dark excitons, A_d - and B_d -, are commonly considered optically forbidden due to the implied violation of the spin selection rule. However, while the B_d -, is noncontroversial strictly dipole forbidden,^{14,25} recent group theory analysis suggests that the restriction upon A_d - can be dismantled by considering out-of-plane dipole transitions.^{14,18,25–27} This dark channel was experimentally demonstrated in various ways, such as surface plasmons polaritons coupling^{28,29} and applied in-plane magnetic fields mixing.^{30–32} Yet, due to the limited strength of its out-of-plane (z -direction) dipoles, it does not yield significant PL at room temperature in comparison with its bright counterparts. Nevertheless, the existence of these dark excitonic states has an acute implication on the material optical signature, arising from the different ordering between the A_d - and A_b - excitons.^{33–36} For example, in different TMDs with chemical compound such as Mo- (W-), the PL is quenched (enhanced) at elevated temperature due to the thermal-population of the dark (bright) excitonic state.^{36,37} Although the delicate thermal stabilization and the A_b -, B_b -exchange interaction has been studied in different TMDs, the possible coupling between the A_d -channel to the B_b -excitonic channel was not demonstrated.

In this work, we report a novel approach to manipulate the bright excitonic channels in MoX_2 -based monolayers, exploiting the excitation of the A_d -state at room temperature. Through control over the out-of-plane component of the excitation electric field, one can select whether to uplift the excitonic population of either the A_b - or the B_b -states, ultimately, encoding the polarization information into the two bright spectral channels (Fig. 1b). Particularly, substantial out-of-plane excitation is used to generate A_d -excitons (Fig. 1e), followed by a surprisingly strong B_b -emission (Fig. 1f) mediated by an ascribed excitonic exchange interaction. In contrast, purely in-plane dipole excitation populates mostly the A_b -excitonic state (Fig. 1c), resulting in its predominant emission (Fig. 1d). By combining the robust optical excitation, thermal role and inherent excitonic exchange interactions, we accomplish polarization information multiplexing into the spectral A_b - and B_b -excitonic channels. Finally, we deduce by *ab initio* calculations and experimental observation exciton mixing of high-energy A_d - and low-lying B_b -states, explaining the higher probability for their coupling in monolayer $MoSe_2$ compared to WSe_2 , which enables (inhibits) the multiplexing operation in Mo- (W-) based monolayer TMDs.

Results and discussion

Emergence of B_b -exciton mediated by dark excitonic transition

The dark excitonic transition depicts the selective excitation of A_d -excitons through the application of out-of-plane polarization.

In monolayer MoX_2 , the formation of this dark exciton mediates the recombination of the B_b -channel, which we theoretically rationalize by an efficient intravalley exciton exchange interactions, based on *ab initio* calculations of the electron-hole transitions, within the GW and Bethe Salpeter equation (GW-BSE) approach and as recently shown for bright A–B exciton coupling.²⁴ Realization of substantial electric field polarization in the z -direction (propagation axis) can be achieved by employing a high numerical aperture (NA) in a high-confocal microscope. Here, the electrical field spatial distribution of the in- and out-of-plane polarizations varies significantly along the propagation axis (Fig. 3a and b), promoting a focal plane based selective excitation of in- and out-of plane dipoles, generating bright and dark excitons, respectively.^{38,39} To experimentally demonstrate the principle of the mechanism, a CVD grown MoS_2 monolayer was transferred onto a 300 nm SiO_2/Si substrate. Continuously excited by an off-resonance 532 nm linearly polarized laser, PL measurements were carried using a high NA objective of 0.75 at different focal planes in a confocal microscope. As a result, a significant wavelength multiplexing of the measured PL spectra (*i.e.* anti-correlated change in the magnitude of the two predominant peaks at around 670 and 620 nm) involving the A_b - and B_b -channels, was achieved by the continues change in the focal plane (Fig. 2a). In comparison, for a low NA objective of 0.25, where the electric field polarization in the z -direction is considerably lower, the transition between the two excitonic states was not observed (Fig. 2b). This implies that the multiplexing occurs due to the alteration of selective excitation of the in- and out-of plane dipoles.

To demonstrate the connection between the dark exciton transition and the B_b -emission, we calculated the spatial distribution of the electric field by numerically solving the Debye–Wolf integral for a linearly x -polarized Gaussian beam.⁴⁰ The electric field amplitude components of $|E_x|$ and $|E_z|$ for NA of 0.75 are depicted in Fig. 3a and b respectively, showing a ratio of 3 : 1 for the max amplitude of $|E_x|:|E_z|$ at the focal point. For comparison, the same simulation was performed for NA of 0.25 (Fig. 3c and d), exhibiting a significantly higher ratio of 10 : 1 between the electric fields of $|E_x|$ and $|E_z|$. The relation between the integrated z -field intensity I_z of an area of 2λ around the optical axis and the B_b -exciton emission (integrated fitted Gaussian B_b -exciton PL peak, normalized to the integrated maximum of the set) at different focal planes are presented in Fig. 3e. A clear correlation between the out-of-plane electric field polarization and the B_b -exciton emission is demonstrated, where the maximum signal of the B_b -exciton is achieved at the focal plane.

Considering that the dark transition prompts the population of the A_d -excitonic state, the relation to the observed B-emission feature can be explained by several excitonic interaction routs, which occur on a faster timescale than the A_d -lifetime,³⁰ such as intravalley excitonic exchange,²⁴ intervalley momentum-forbidden excitonic interaction³³ and the formation of charged excitons.^{41–44} The latter, however, can be excluded due to the lack of alteration in the B-signal under gate bias (see ESI† note 2); while an interplay between the neutral and charged excitons

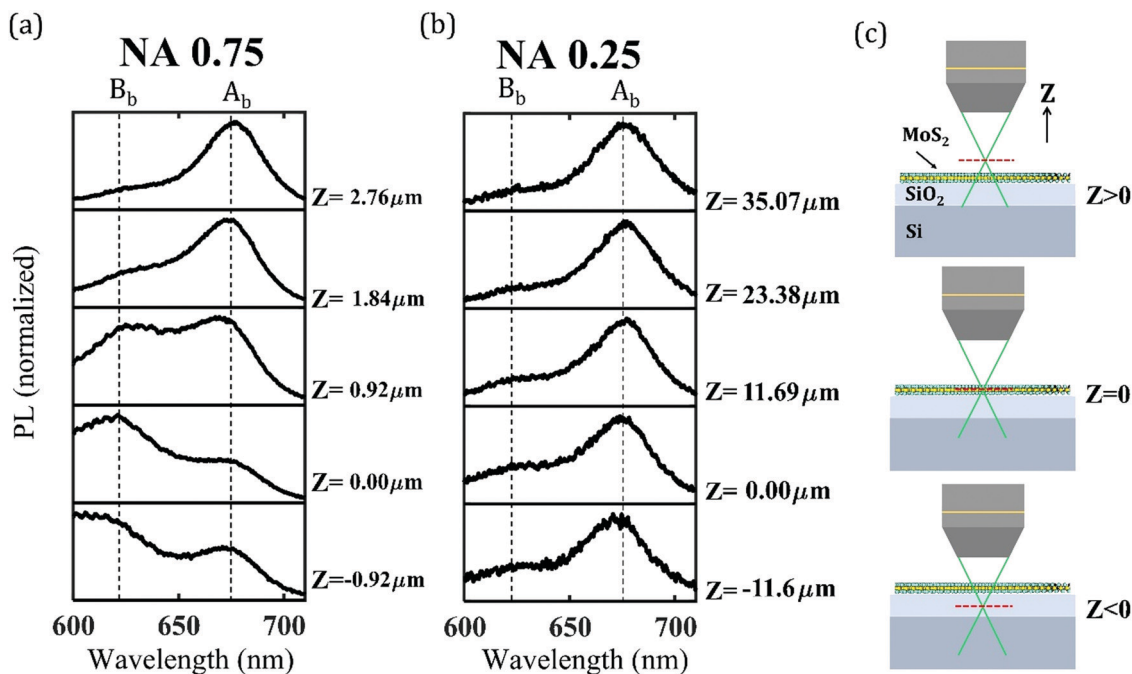


Fig. 2 In-plane and out-of-plane PL dependent excitation. (a) Measured PL spectra of MoS₂ for different focal planes, taken with high NA (0.75) objective showing a clear transition between A_b- and B_b-emission as function of the focal plane position. (b) Measured PL spectra of MoS₂ for different focal planes, taken with a low NA (0.25) objective showing no excitonic transition. (c) Schematic illustration of the experimental setup, the objective is moved to different focal planes (dashed red line), where the z-axis origin is determined to be at the focal plane overlapping with the MoS₂ monolayer.

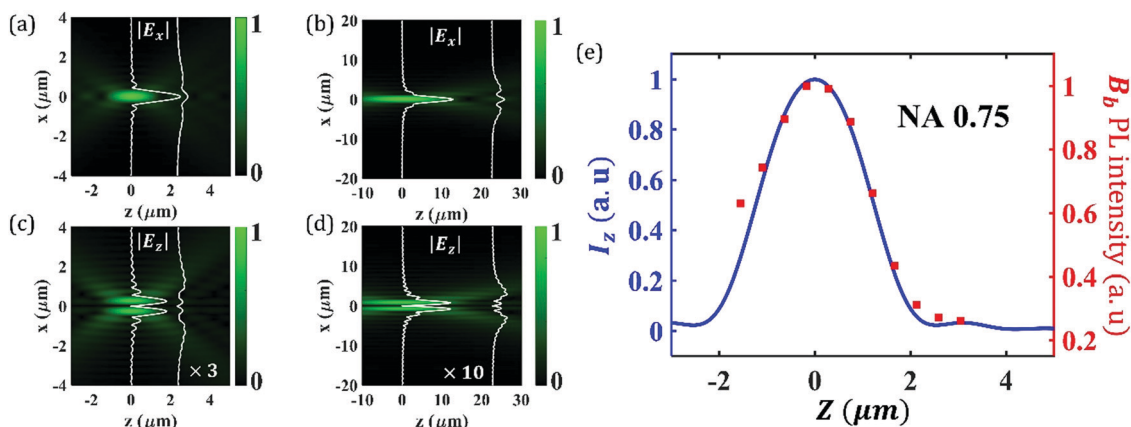


Fig. 3 PL dependence on In-plane and out-of-plane excitation. (a and b) Calculated electric field in the xz-plane of a propagating Gaussian beam for a high NA of 0.75 objective. The max amplitude ratio received for $|E_x|:|E_z|$ is approximately 3:1 indicating that a significant contribution to out-of-plane dipole excitation is feasible. The white lines indicate the spatial amplitude distribution at different focal planes. (c and d) Similar calculated electric fields for a low NA of 0.25 objective. Here, we find a considerably lower ratio between the $|E_x|:|E_z|$ of around 10:1. (e) Correlation between the integrated z-field intensity I_z for an area of 2λ around the optical axis and the B_b-excitonic contribution (integrated Gaussian signal) from the general spectrum. Both I_z and the B_b-contribution were normalized to the set value at $z = 0$. We note that the B_b-contribution set was slightly shifted by 0.17 (μm) to have better overlapping with the field intensity.

can be observed for the A-exciton regime. Additionally, the population of the A_b- seems to increase by the application of positive voltage with no apparent change of the B-emission, indicating a less effective bright-to-bright intravalley excitonic exchange.^{20,24} While intervalley interaction has been shown to be prudent in the optical behavior of monolayer TMDs, it is mostly emphasized in the context of the B_b-bleaching.^{34,45} Thus, we

connect the increase of the B-emission feature to the B_b-exciton *via* an unexplored dark mediated excitonic transition, as will be shown below.

As aforementioned, out-of-plane excitation promotes the excitonic population of the higher energetic dark state in monolayer MoS₂, which is followed by the strong B_b-excitonic emission. Nonetheless, such dark states can decay non-radiatively through

intravalley scattering, leading to the bleaching of the B_b -excitonic state and increase in A_b -emission.^{24,34,46,47} Since the intravalley scattering time τ_{bd} occurs on a faster time scale than the radiative recombination $\tau_{bd} \ll \tau_{Ad}, \tau_{Ab}, \tau_{Bb}$,^{48,49} thermal equilibrium has a major role in determining the population distribution within the excitonic levels. We therefore expect that at low (high) temperatures, a strongly populated lower (higher) excitonic level, will result in strong A_b - (B_b -) exciton emission. Evidently, strong A_b - exciton emission was recently observed in monolayer MoSe_2 at low temperatures, albeit excitation was induced by out-of-plane polarization.²⁵

Thermal dependent photoluminescence

To study the thermal dependency of the above excitonic multiplexing, we conducted PL measurements at temperatures range of 125–298 K using a THMS600 cooling system (LinKam Ltd.) and an objective with NA of 0.45 to account for the increased

working distance. Fig. 4a and b present the PL measurements at different focal planes for the two temperatures extrema *i.e.* at 298 K and at 125 K, showing a substantial reduction in the B_b -excitonic emission channel at low temperature. We first consider a simplified excitonic picture, which does not include exchange interactions between the A and B transitions, where both the A_d - and B_b -excitonic energy levels lie above the A_b - and B_d -levels, respectively; thus, thermal scattering may impose higher populations of the B_b - and A_d -states, as schematically demonstrated in Fig. 4c (see ESI† note 3). However, such simplified explanation is not enough to understand the origin of the modulation without an exchange-driven interaction, as we further explore below, since thermal energy alone cannot surpass the 150 meV energetic barrier between the excitonic species (Fig. 4c). With that in mind, the ratio between the B_b - and A_b -emission can be naively described by an Arrhenius relation for the intravalley scattering between the A- and B-states.

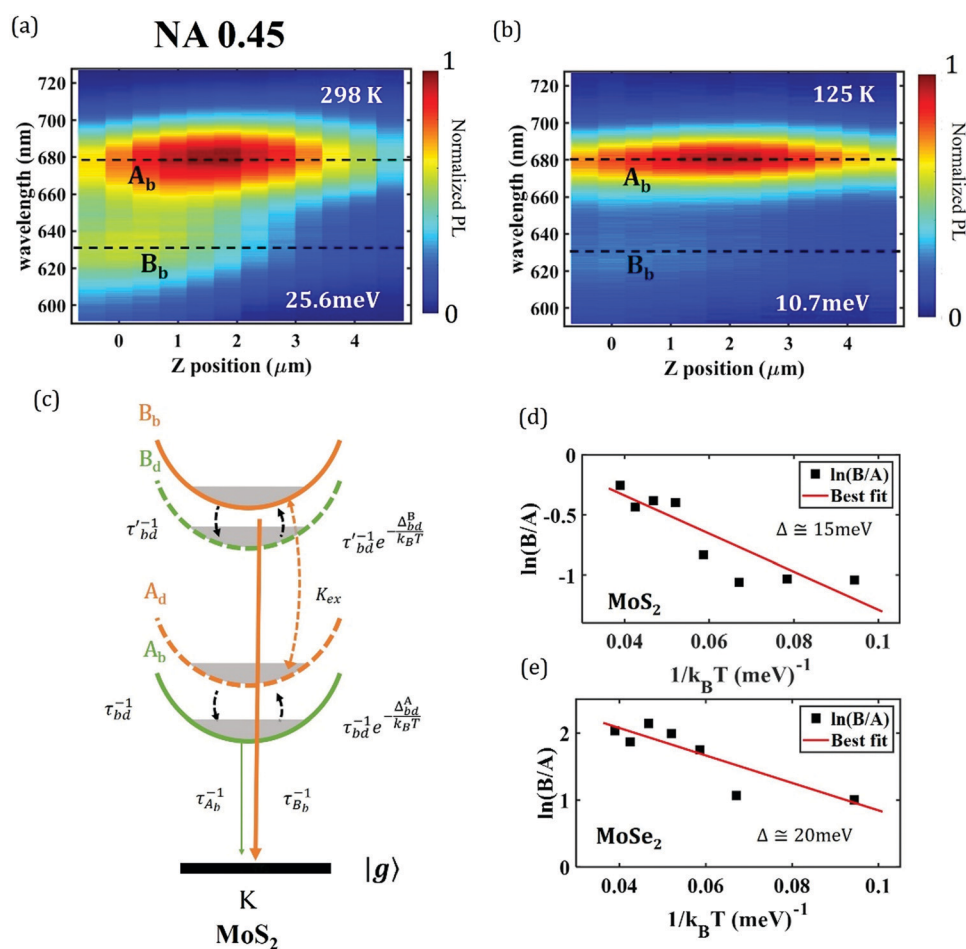


Fig. 4 Temperature dependent PL modulation. Measured normalized PL colormap of monolayer MoS_2 taken with a NA of 0.45 for different focal planes at 298 K (a) and 125 K (b). The spectra were normalized for the maximum value of the measurement set at a given temperature. The thermal energy $k_B T$ is marked on the bottom right in each spectrum. The B_b -excitonic emission is observed at high temperatures, whereas at low temperatures the exciton emission is quenched. (c) Schematic of intravalley non-mixed excitonic states in MoS_2 . Dashed lines represent dark transitions, band color represent correlating CB band transition (upper CB-orange; lower CB- green). Here the K_{ex} depicts the excitonic mixing of the dark (A_d)-to-bright (B_b -) exchange. (d and e) Relative PL integrated intensity between the A_b - and B_b -excitonic emission for MoS_2 and MoSe_2 , respectively. The intensities are taken in a natural logarithm as a function of $(k_B T)^{-1}$ marked by the black squares. The results were fitted with the thermal scattering model presented in the text marked by the red line with a slope of $\Delta \cong 15$ and $\Delta \cong 20$ (meV) for MoS_2 and MoSe_2 , respectively.

Here, under an assumption that the A_d - emission is negligible with respect to the intravalley scattering, the excitonic population ratio can be represented as $B/A \propto \exp(-\Delta/k_B T)$. Where Δ is the thermal activation energy, k_B is the Boltzmann constant and A and B correspond to the population of the A_b - and B_b -excitonic population, respectively. This relation corresponds to the linear behavior between $\ln(B_b/A_b)$ (integrated intensities of the B_b - and A_b -emission) taken at $z = 0$ and $1/k_B T$ (Fig. 4d). Indeed, the extracted activation energy of ~ 15 meV is not sufficient to explain direct transitions between the A and B exciton onset, and demands a more complicated dynamical effects, as we elaborate below.

To examine the generality of this phenomenon, similar temperature dependent PL measurements were conducted for monolayer MoSe_2 placed on a 300 nm SiO_2/Si substrate (see ESI† note 3). Similar multiplexing of the B_b - and A_b -channels was observed, while MoSe_2 presented larger B_b/A_b excitonic emission ratio that can be attributed to its rapid valley depolarization, stronger B_b -momentum dipole transition⁵⁰ and comparable stronger mixing rates.²⁴ Additionally, the temperature dependent PL spectra of MoSe_2 are in correspondence with the Arrhenius relation of $\Delta \cong 20$ meV (Fig. 4e). These results demonstrate the importance of thermal energy for realizing strong B_b -excitonic emission mediated by the dark exciton transition. The discrepancy between the observed thermal barrier of ~ 10 – 20 meV and the significantly larger energy difference between the A_d and the B_b energies (> 100 meV) suggest that the excited A_d excitons involve high energetic level states, *i.e.* X_2 , corresponding to the broadband excitation in our setup (2.33 eV). Such high energetic excitation is sufficient to directly populate A_d

excitons with high enough energy to mediate the strong B_b emission, as will be shown below. We also note that the similar observed response for different MoX_2 monolayers suggests a common mechanism that originates from their profound exciton mixing, as we show in the next sections. It is also important to note that similar trend in modulation of B_b/A_b exciton emission ratio is expected due to chromatic aberration, which similarly separates frequencies into different focal plains.⁵¹ Importantly, the chromatic aberration in the spectral range of the A_b - and B_b - was found to be minor in our setup (see ESI† note 5).

We further compare between PL measurements of MoSe_2 (Fig. 5a) and WSe_2 (Fig. 5b), both placed on a 300 nm SiO_2/Si substrate and measured with a NA of 0.75. Interestingly, a significantly weaker multiplexing of the B_b/A_b ratio is observed for WSe_2 in comparison with MoSe_2 . These findings point to exciton coupling mechanisms that depend in both the energy and the coupling probabilities between the participating excitons, as we discuss below.

Dark-to-bright exciton mixing in MoSe_2 and WSe_2

To understand the mechanism dominating the observed dark-to-bright exciton transitions, we analyze plausible exciton interaction mechanisms. First, we consider single-exciton state coupling due to intravalley exchange interactions, as was recently demonstrated in MoS_2 .²⁴ We performed many-body perturbation theory calculations within the GW-BSE approximation, while explicitly including spinor wavefunctions of the electron and hole states. This method allows a close inspection of the various electron-hole transitions contributing to the excitonic states in the energy range of the explored A and B peaks. In particular, we

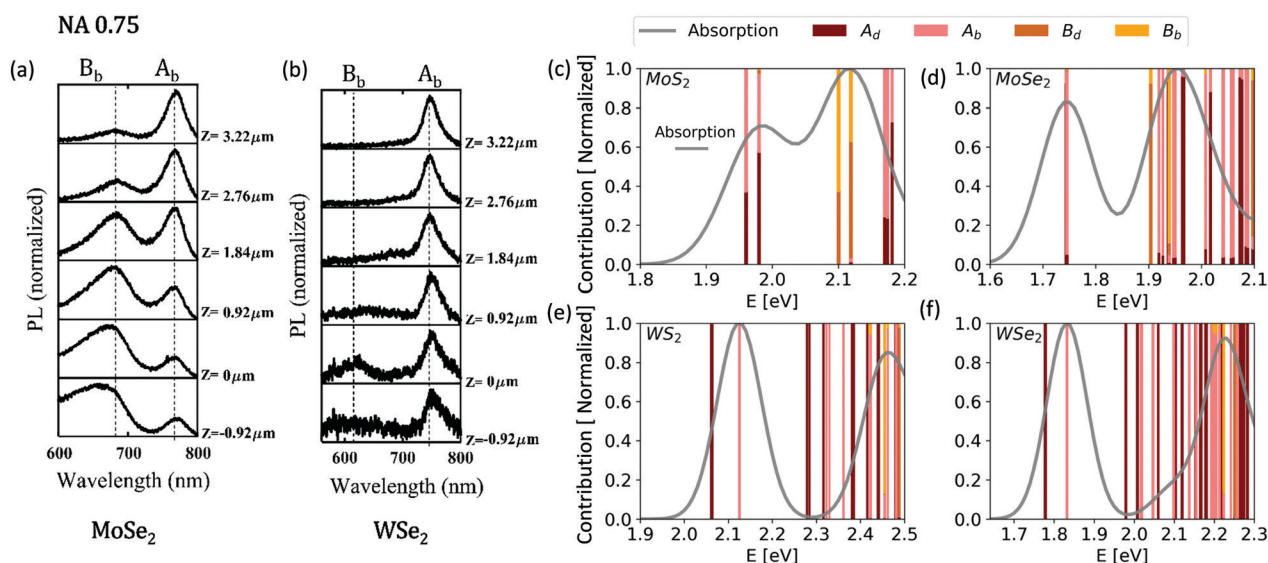


Fig. 5 Excitonic mixing in TMDCs and PL excitonic modulation. (a and b) Room temperature PL spectra taken with a NA of 0.75 at different focal planes for MoSe_2 and WSe_2 , respectively. The observed excitonic modulation is profound in MoSe_2 , while very small in WSe_2 . (c–f) Computed GW-BSE absorption spectra and the respective contributing exciton transitions for MoS_2 , MoSe_2 , WS_2 , and WSe_2 monolayers, respectively. Different colors represent the fraction of the normalized contributions from A_b -, A_d -, B_b -, B_d -transitions as defined in the text. Comparing between the examined systems, MoS_2 and MoSe_2 (c and d) have significantly larger mixing between bright and dark transitions than WS_2 and WSe_2 (e and f), where hardly any mixing occurs. In addition, while in the Mo-based monolayers the B_b -state appears close in energy and slightly below the second A excitation, in the W-based systems they appear around higher A excitations, reducing the probability to be occupied by optically excited A states.

study the exciton mixing level of the A_b , A_d , B_b , and B_d states, for MoS_2 , $MoSe_2$, WS_2 , and WSe_2 (Fig. 5c–f). For MoS_2 and $MoSe_2$ we find that A exciton states strongly mix dark and bright electron–hole transitions, and slightly mix with B states, in good correspondence with previous observations.²⁴ Importantly, higher-energy mixed (dark–bright) A exciton states are also found slightly above the spin-split bright B peak in both systems (full data of state mixing is given in the ESI† note 6). Our results point to possible decay channels which can eventually explain the modulated B_b emission. In this scenario, in both MoS_2 and $MoSe_2$, excited-state absorption can populate mixed A_d - and A_b -exciton states, which in turn couple to mixed B_d - and B_b -states. Such coupling is allowed due to intervalley exchange mixing, as shown by Guo *et al.*²⁴ and in our present calculations. In stark contrast, the excitonic picture in WSe_2 and WS_2 reveals a very different mixing nature: the computed low-energy A excitations are well separated and do not mix dark and bright nature. In addition, due to the large SOC energy split, the B_b exciton energetically coincide with much higher excited A states, lowering the decay probability to the low-energy B_b -exciton.

Considering the relatively low effective thermal barrier that is extracted from the temperature dependent PL measurements, it is plausible that excited-state A excitons thermally couple to low-lying B excitons *via* absorption or emission of phonons with energies at the scale of ~ 10 – 60 meV before they optically decay. Such relaxation mechanism can be associated with previously-observed phonon-assisted dark exciton decay processes^{34,52–54} with exciton coupling allowed due to exchange mixing. A second scenario, although less plausible, involves an upconversion mechanism from the lowest, X_1 exciton state, partially dominated by A_d transitions, to the higher X_2 exciton state, dominated by B_b transitions. Such exciton–exciton coupling must overcome energy differences at the order of 150 meV in Mo-based monolayers, and 300 meV in the W-based ones. This channel may be associated to a recently-suggested upconversion process between bright A and B states in WSe_2 , observed in PLE measurements, and related with non-linear processes such as phonon-assisted Auger recombination.⁴⁶ To explore this further, PL resonant excitation measurements were carried out with monolayer MoS_2 (ESI† Fig. S8). Here, under excitation of 633 nm at different focal planes the B-excitonic signal was not observed, making the upconversion process a less plausible exchange route compared to the coherent exchange interaction in the 2s region. This indicates the pivotal role of the exchange interaction and specifically, the part of the dark-to-bright exchange channels, arising from out-of-plane excited A_d -related states for the amplification of the B_b -signal. We thus attribute these bright-to-dark exchange channels as the predominant mechanism for the multiplexing action in MoX_2 TMDs monolayers. The computed exciton mixing is much weaker for the case of WS_2/WSe_2 , offering a possible explanation for our experimental findings of reduced B_b/A_b transition probabilities (Fig. 5b). Finally, there are still several key questions that one has to address in order to get a quantitative understating regarding the quantum efficiency of such dark to bright excitonic transition. In particular, the selective high-energy excitonic absorption (dark and bright) as a function

of light polarization (longitudinal *vs.* transverse) and their correlation with the resulting PL emission.

Conclusions

In summary, we demonstrate a new approach for bright excitons multiplexing of the A_b - and B_b -excitonic channels in monolayer TMDs at room temperature. As a proof of concept, dark excitonic mediated transitions were realized by a confocal microscope with high NA. Thus, selective excitation of high energy A_d -excitons were observed at different focal planes, mediating the emission of the B_b -exciton channel *via* dark-to-bright exchange interactions. Furthermore, we establish the important role of excitonic thermal scattering and excitonic ordering. Finally, GW-BSE calculations were employed to unveil profound exciton state mixing and coupling in MoX_2 compared with WX_2 , which ultimately enables the multiplexing operation. These findings shed light on the fundamental optical properties of monolayer TMDs, while paving a novel route for TMDs based photonic devices, *e.g.* spectral bits for optical computing, multi-functional and tunable light sources and more.

Materials and methods

Sample preparation

MoS_2 and $MoSe_2$ monolayers were grown by a space confined CVD approach, as previously reported.^{55,56} In a typical growth process, MoO_3 (99.5%, Sigma Aldrich) and Sulfur (or Selenium) powders (99.95%, Sigma Aldrich) were used as the metal and the chalcogen precursors, respectively. A ceramic boat containing (~ 3.5 mg) of MoO_3 powder was placed at the center of a 1-inch diameter CVD furnace. A piece of 300 nm thermally grown SiO_2 coated Si substrate was mounted on top of the same boat with its polished surface facing upwards. Few small pieces of mica sheets were cut and placed above the target substrate. The Sulfur (or Se, ~ 350 mg) boat was placed ~ 22 cm upstream from the MoO_3 source-growth substrate. The quartz tube was initially purged with ~ 250 sccm of highly pure Ar (5N) carrier gas for 10 minutes. Thereafter, the furnace temperature was ramped to 750 °C at 15 °C per minute with 30 sccm of Ar flow and the chalcogen was separately heated to 150 °C or 240 °C, for S and Se, respectively. The growth time was kept for 5–10 minutes at 750 °C. MoS_2 and $MoSe_2$ samples were then wet-transfer to the SiO_2/Si substrate: The TMDs monolayers were spin coated with 0.5 wt% polystyrene (PS) for 60 seconds at 4000 rpm, followed with two baking steps at 90 °C for 35 minutes and 120 °C for 15 minutes. The samples were then placed in DI for 5 minutes until the PS-TMDs film was malleable enough to peel from the substrate. The film was taken out with the Si/SiO_2 substrate and baked with the same previous conditions. Finally, toluene was used to dissolve the PS film. The highly crystalline grown CVD WSe_2 sample was commercially acquired (2D semiconductors) and was mechanically transferred to a SiO_2/Si substrate.

Optical measurements. PL measurements were conducted using a WITec alpha 300R confocal Raman microscopy system;

with excitation power intensity of 0.5 mW from a single fiber mode 532 nm linear polarized laser. The PL was acquired using a 600 g mm⁻¹ grating. Measurements at different focal planes were conducted by moving the objective position in z-axis. The objectives used in the experiment include: 10x/0.25, 50x/0.75 by Zeiss and 50x/0.45 by Olympus. Thermal measurements were conducted using a LinKam THMS600 temperature-controlled chamber. For convenience, the experimental zero position of the focal plane is set according to the strongest received B₁-exciton signal (Fig. 2c).

Theoretical calculations

We obtain the starting point electron and hole wavefunctions from density functional theory (DFT)⁵⁷ calculations within the PBE approximation,⁵⁸ using the Quantum Espresso package.⁵⁹ We use a 2D periodic unit cell with lattice vectors of 3.29 Å for MoSe₂ and WSe₂ and 3.16 Å for MoS₂ and WS₂, with a 15 Å distance between repeating unit cells in the out-of-plane direction. We apply a plane-wave basis and norm-conserving pseudopotentials. A 30 × 30 × 1 *k*-point grid was used to calculate the self-consistent charge density with a 70 Ry wave function cutoff. Spin polarization was included using fully-relativistic corrections. We compute the quasiparticle band structure using the GW method within the BerkeleyGW software⁵⁸ using the Hybertsen–Louie generalized plasmon-pole (HL-GPP) model.^{60,61} We used a screening energy cutoff of 25 Ry for the reciprocal lattice components of the dielectric matrix and included 4000 spinor bands in the summation. We employed the nonuniform neck subsampling (NNS) scheme⁶² to sample the Brillouin zone. In this scheme, we use a 6 × 6 × 1 uniform *q*-grid and include an additional set of 10 *q*-points in the Voronoi cell around *q* = 0. A truncated Coulomb interaction was used to prevent spurious interactions between periodic images of the 2D sheet.⁶³ We solve the Bethe Salpeter equation (BSE) for the spinor electron and hole wavefunctions within the Tamm–Dancoff approximation (TDA), as implemented in the BerkeleyGW code.^{60,64} The BSE matrix elements were calculated on a uniform 24 × 24 × 1 *k*-grid and then interpolated to a 48 × 48 × 1 fine *k*-grid, with 6 empty and 6 occupied bands included in the transition matrix.

Data availability

The data that support the findings of this study are available from the corresponding author upon reasonable request.

Author contributions

S. K. B. C. and E.K. conceived the experimental concept. S.K. and S.M. performed the experimental work. B. C. and S. S. performed optical calculations. P. M. and A. P. performed CVD growth of 2D samples. S. R. A. and T. A. performed the *ab initio* calculations. V. K., A. I., S. R. A., E. H. and E. K. supervised the work. All authors participated in the data analysis and in the writing of the manuscript.

Conflicts of interest

The authors declare no competing interests.

Acknowledgements

E. K. gratefully acknowledge the Israel Science Foundation (ISF), grant 1567/18, for financial assistance and the RBNI for the nanofabrication facilities. E. K. thanks the Taub fellowship for leadership in science and technology, supported by the Taub Foundation and the Alon fellowship. E. H. gratefully acknowledge the Israel Science Foundation (ISF), the US Air Force Office of Scientific Research (FA9550-18-1-0208) through their program on Photonic Metamaterials and the Israel Ministry of Science, Technology and Space. S. R. A. acknowledges support from the Israel Science Foundation (ISF) Grant No. 1208/19 and an Alon Fellowship. P. K. M. and A. I. acknowledge the generous support from the Israel Science Foundation, projects # 2549/17 and 2171/17. This research used computational resources of the National Energy Research Scientific Computing Center (NERSC). This research used computational resources of the National Energy Research Scientific Computing Center (NERSC) and of the ChemFarm Computational Cluster at the Weizmann Institute.

References

- 1 G. D. Scholes and G. Rumbles, *Materials For Sustainable Energy: A Collection of Peer-Reviewed Research and Review Articles from Nature Publishing Group*, 2011, 12–25.
- 2 K. F. Mak, C. Lee, J. Hone, J. Shan and T. F. Heinz, *Phys. Rev. Lett.*, 2010, **105**, 136805.
- 3 K. He, N. Kumar, L. Zhao, Z. Wang, K. F. Mak, H. Zhao and J. Shan, *Phys. Rev. Lett.*, 2014, **113**, 026803.
- 4 A. Splendiani, L. Sun, Y. Zhang, T. Li, J. Kim, C.-Y. Chim, G. Galli and F. Wang, *Nano Lett.*, 2010, **10**, 1271–1275.
- 5 K. Rong, B. Wang, A. Reuven, E. Maguid, B. Cohn, V. Kleiner, S. Katznelson, E. Koren and E. Hasman, *Nat. Nanotechnol.*, 2020, **15**, 927–933.
- 6 M. Koperski, M. R. Molas, A. Arora, K. Nogajewski, A. O. Slobodeniuk, C. Faugeras and M. Potemski, *Nanophotonics*, 2017, **6**, 1289–1308.
- 7 F. Xia, H. Wang, D. Xiao, M. Dubey and A. Ramasubramaniam, *Nat. Photonics*, 2014, **8**, 899–907.
- 8 D. Xiao, G.-B. Liu, W. Feng, X. Xu and W. Yao, *Phys. Rev. Lett.*, 2012, **108**, 196802.
- 9 W. Zhao, Z. Ghorannevis, L. Chu, M. Toh, C. Kloc, P.-H. Tan and G. Eda, *ACS Nano*, 2013, **7**, 791–797.
- 10 A. Kormányos, G. Burkard, M. Gmitra, J. Fabian, V. Zólyomi, N. D. Drummond and V. Fal'ko, *2D Mater.*, 2015, **2**, 022001.
- 11 X. Xu, W. Yao, D. Xiao and T. F. Heinz, *Nat. Phys.*, 2014, **10**, 343–350.
- 12 K. Kośmider, J. W. González and J. Fernández-Rossier, *Phys. Rev. B: Condens. Matter Mater. Phys.*, 2013, **88**, 245436.
- 13 G.-B. Liu, W.-Y. Shan, Y. Yao, W. Yao and D. Xiao, *Phys. Rev. B: Condens. Matter Mater. Phys.*, 2013, **88**, 085433.
- 14 J. Echeverry, B. Urbaszek, T. Amand, X. Marie and I. Gerber, *Phys. Rev. B*, 2016, **93**, 121107.

- 15 A. Slobodeniuk and D. Basko, *2D Mater.*, 2016, **3**, 035009.
- 16 T. Mueller and E. Malic, *npj 2D Mater. Appl.*, 2018, **2**, 29.
- 17 J. Xiao, M. Zhao, Y. Wang and X. Zhang, *Nanophotonics*, 2017, **6**, 1309–1328.
- 18 Z. Ye, T. Cao, K. O'Brien, H. Zhu, X. Yin, Y. Wang, S. G. Louie and X. Zhang, *Nature*, 2014, **513**, 214–218.
- 19 J. A. Schuller, S. Karaveli, T. Schiros, K. He, S. Yang, I. Kymissis, J. Shan and R. Zia, *Nat. Nanotechnol.*, 2013, **8**, 271.
- 20 Y.-C. Wu, S. Samudrala, A. McClung, T. Taniguchi, K. Watanabe, A. Arbabi and J. Yan, *ACS Nano*, 2020, **14**, 10503–10509.
- 21 S. Dubey, S. Lisi, G. Nayak, F. Herzig, V.-D. Nguyen, T. Le Quang, V. Cherkez, C. Gonzalez, Y. J. Dappe and K. Watanabe, *ACS Nano*, 2017, **11**, 11206–11216.
- 22 M. Buscema, G. A. Steele, H. S. van der Zant and A. Castellanos-Gomez, *Nano Res.*, 2014, **7**, 561–571.
- 23 K. M. McCreary, A. T. Hanbicki, S. V. Sivaram and B. T. Jonker, *APL Mater.*, 2018, **6**, 111106.
- 24 L. Guo, M. Wu, T. Cao, D. M. Monahan, Y.-H. Lee, S. G. Louie and G. R. Fleming, *Nat. Phys.*, 2019, **15**, 228–232.
- 25 G. Wang, C. Robert, M. Glazov, F. Cadiz, E. Courtade, T. Amand, D. Lagarde, T. Taniguchi, K. Watanabe and B. Urbaszek, *Phys. Rev. Lett.*, 2017, **119**, 047401.
- 26 M. R. Molas, A. O. Slobodeniuk, T. Kazimierzczuk, K. Nogajewski, M. Bartos, P. Kapuifmmode, K. Oreszczuk, K. Watanabe, T. Taniguchi, C. Faugeras, P. Kossacki, D. M. Basko and M. Potemski, *Phys. Rev. Lett.*, 2019, **123**, 096803.
- 27 L. M. Schneider, S. S. Esdaille, D. A. Rhodes, K. Barmak, J. C. Hone and A. Rahimi-Iman, *Sci. Rep.*, 2020, **10**, 1–6.
- 28 K.-D. Park, T. Jiang, G. Clark, X. Xu and M. B. Raschke, *Nat. Nanotechnol.*, 2018, **13**, 59–64.
- 29 Y. Zhou, G. Scuri, D. S. Wild, A. A. High, A. Dibos, L. A. Jauregui, C. Shu, K. De Greve, K. Pistunova and A. Y. Joe, *Nat. Nanotechnol.*, 2017, **12**, 856.
- 30 X.-X. Zhang, T. Cao, Z. Lu, Y.-C. Lin, F. Zhang, Y. Wang, Z. Li, J. C. Hone, J. A. Robinson and D. Smirnov, *Nat. Nanotechnol.*, 2017, **12**, 883–888.
- 31 C. Robert, B. Han, P. Kapuscinski, A. Delhomme, C. Faugeras, T. Amand, M. Molas, M. Bartos, K. Watanabe and T. Taniguchi, *Nat. Commun.*, 2020, **11**, 1–8.
- 32 Z. Lu, D. Rhodes, Z. Li, D. Van Tuan, Y. Jiang, J. Ludwig, Z. Jiang, Z. Lian, S.-F. Shi and J. Hone, *2D Mater.*, 2019, **7**, 015017.
- 33 E. Malic, M. Selig, M. Feierabend, S. Brem, D. Christiansen, F. Wendler, A. Knorr and G. Berghäuser, *Phys. Rev. Mater.*, 2018, **2**, 014002.
- 34 M. Selig, F. Katsch, R. Schmidt, S. M. de Vasconcellos, R. Bratschitsch, E. Malic and A. Knorr, *Phys. Rev. Res.*, 2019, **1**, 022007.
- 35 M. R. Molas, C. Faugeras, A. Slobodeniuk, K. Nogajewski, M. Bartos, D. Basko and M. Potemski, *2D Mater.*, 2017, **4**, 021003.
- 36 X.-X. Zhang, Y. You, S. Y. F. Zhao and T. F. Heinz, *Phys. Rev. Lett.*, 2015, **115**, 257403.
- 37 G.-H. Peng, P.-Y. Lo, W.-H. Li, Y.-C. Huang, Y.-H. Chen, C.-H. Lee, C.-K. Yang and S.-J. Cheng, *Nano Lett.*, 2019, **19**, 2299–2312.
- 38 M. Brotons-Gisbert, R. Proux, R. Picard, D. Andres-Penares, A. Branny, A. Molina-Sánchez, J. F. Sánchez-Royo and B. D. Gerardot, *Nat. Commun.*, 2019, **10**, 1–10.
- 39 R. Scott, J. Heckmann, A. V. Prudnikau, A. Antanovich, A. Mikhailov, N. Owschimikow, M. Artemyev, J. I. Climente, U. Woggon and N. B. Grosse, *Nat. Nanotechnol.*, 2017, **12**, 1155–1160.
- 40 E. Wolf, *Proc. R. Soc. London, Ser. A*, 1959, **253**, 349–357.
- 41 K. F. Mak, K. He, C. Lee, G. H. Lee, J. Hone, T. F. Heinz and J. Shan, *Nat. Mater.*, 2013, **12**, 207–211.
- 42 J. Förste, N. V. Tepliakov, S. Y. Kruchinin, J. Lindlau, V. Funk, M. Förg, K. Watanabe, T. Taniguchi, A. S. Baimuratov and A. Högele, *Nat. Commun.*, 2020, **11**, 1–8.
- 43 K. Shinokita, X. Wang, Y. Miyauchi, K. Watanabe, T. Taniguchi, S. Konabe and K. Matsuda, *Phys. Rev. B*, 2019, **99**, 245307.
- 44 Brill, *ACS Appl. Mater. Interfaces*, 2021, **13**(27), 32590–32597.
- 45 G. Berghäuser, I. Bernal-Villamil, R. Schmidt, R. Schneider, I. Niehues, P. Erhart, S. M. de Vasconcellos, R. Bratschitsch, A. Knorr and E. Malic, *Nat. Commun.*, 2018, **9**, 1–8.
- 46 M. Manca, M. Glazov, C. Robert, F. Cadiz, T. Taniguchi, K. Watanabe, E. Courtade, T. Amand, P. Renucci and X. Marie, *Nat. Commun.*, 2017, **8**, 1–7.
- 47 Z. Wang, A. Molina-Sanchez, P. Altmann, D. Sangalli, D. De Fazio, G. Soavi, U. Sassi, F. Bottegoni, F. Ciccacci and M. Finazzi, *Nano Lett.*, 2018, **18**, 6882–6891.
- 48 K. F. Mak, K. He, J. Shan and T. F. Heinz, *Nat. Nanotechnol.*, 2012, **7**, 494–498.
- 49 L. Yang, N. A. Sinitsyn, W. Chen, J. Yuan, J. Zhang, J. Lou and S. A. Crooker, *Nat. Phys.*, 2015, **11**, 830–834.
- 50 M. Yang, C. Robert, Z. Lu, D. Van Tuan, D. Smirnov, X. Marie and H. Dery, *Phys. Rev. B*, 2020, **101**, 115307.
- 51 P. Lasch, A. Hermelink and D. Naumann, *Analyst*, 2009, **134**, 1162–1170.
- 52 M. Selig, G. Berghäuser, A. Raja, P. Nagler, C. Schüller, T. F. Heinz, T. Korn, A. Chernikov, E. Malic and A. Knorr, *Nat. Commun.*, 2016, **7**, 1–6.
- 53 D. Christiansen, M. Selig, G. Berghäuser, R. Schmidt, I. Niehues, R. Schneider, A. Arora, S. M. de Vasconcellos, R. Bratschitsch and E. Malic, *Phys. Rev. Lett.*, 2017, **119**, 187402.
- 54 Z. Li, T. Wang, C. Jin, Z. Lu, Z. Lian, Y. Meng, M. Blei, M. Gao, T. Taniguchi and K. Watanabe, *ACS Nano*, 2019, **13**, 14107–14113.
- 55 P. Mohapatra, S. Deb, B. Singh, P. Vasa and S. Dhar, *Appl. Phys. Lett.*, 2016, **108**, 042101.
- 56 P. K. Mohapatra, K. Ranganathan and A. Ismach, *Adv. Mater. Interfaces*, 2020, **7**, 2001549.
- 57 W. Kohn and L. J. Sham, *Phys. Rev.*, 1965, **140**, A1133.
- 58 J. P. Perdew, K. Burke and M. Ernzerhof, *Phys. Rev. Lett.*, 1996, **77**, 3865.
- 59 P. Giannozzi, O. Andreussi, T. Brumme, O. Bunau, M. B. Nardelli, M. Calandra, R. Car, C. Cavazzoni, D. Ceresoli and M. Cococcioni, *J. Phys.: Condens. Matter*, 2017, **29**, 465901.
- 60 J. Deslippe, G. Samsonidze, D. A. Strubbe, M. Jain, M. L. Cohen and S. G. Louie, *Comput. Phys. Commun.*, 2012, **183**, 1269–1289.

- 61 M. S. Hybertsen and S. G. Louie, *Phys. Rev. Lett.*, 1985, **55**, 1418.
- 62 H. Felipe, D. Y. Qiu and S. G. Louie, *Phys. Rev. B*, 2017, **95**, 035109.
- 63 S. Ismail-Beigi, *Phys. Rev. B: Condens. Matter Mater. Phys.*, 2006, **73**, 233103.
- 64 M. Rohlfing and S. G. Louie, *Phys. Rev. B: Condens. Matter Mater. Phys.*, 2000, **62**, 4927.